R-06-115

Demonstrating the efficiency of the EFPC criterion by means of Sensitivity analyses

Raymond Munier, Svensk Kärnbränslehantering AB

April 2007

Svensk Kärnbränslehantering AB
Swedish Nuclear Fuel
and Waste Management Co
Box 5864
SE-102 40 Stockholm Sweden
Tel 08-459 84 00
+46 8 459 84 00
Fax 08-661 57 19
+46 8 661 57 19

ISSN 1402-3091
SKB Rapport R-06-115

Demonstrating the efficiency of the EFPC criterion by means of Sensitivity analyses

Raymond Munier, Svensk Kärnbränslehantering AB

April 2007

Contents

1 Introduction

Within the framework of a project to characterise large fractures /Cosgrove et al. 2006/, a modelling effort was initiated to evaluate the use of a pair of full perimeter criteria, FPC and EFPC /Munier 2006/, for detecting fractures that could jeopardize the integrity of the canisters in the case of a large nearby earthquake.

Though some sensitivity studies were performed in the method study of /Munier 2006/ these mainly targeted aspects of Monte-Carlo simulations. The impact of uncertainties in the DFN model upon the efficiency of the FPI criteria was left unattended.

The main purpose of this report is, therefore, to explore the impact of DFN variability upon the efficiency of the FPI criteria. The outcome of the present report may thus be regarded as complementary analyses to the ones presented in /Munier 2006/. To appreciate the details of the present report, the reader should be acquainted with the simulation procedure described in /Munier 2006/.

2 Analysis setup

The variability and uncertainties in the fracture size distributions have not, in the published SDMs, been explored in such a manner that it can be directly used for sensitivity analysis of canister intersection statistics.

We therefore induced variability by altering some properties of the Forsmark v.1.2. DFN /La Pointe et al. 2005/ which was judged the most appropriate DFN model for the purposes of the present study, mainly because it requires substantially less computation time than the Laxemar or Simpevarp models.

/Hedin 2005/ showed, using an analytical solution, that the orientation of the fracture sets had negligible impact on the canister/fracture intersection statistics. Orientation of fracture sets do, however, impact the intersection probabilities with deposition *tunnels*. We have in the simulations presented here, chosen tunnel orientations as proposed by /Brantberger et al. 2006/.

Though other size distributions have been reported, the Powerlaw (Pareto) distribution has been the most successful in describing fracture sizes at the SKB study sites /Darcel et al. 2004, Hermanson et al. 2005, La Pointe et al. 2005/ which motivated us to restrict the span of the analysis further. The DFN parameters of concern to this study are thus (Table 2-1):

k_r, the shape parameter (slope) of the Pareto distribution

r_0, [m] the location parameter (minimum fracture radius consistent with the DFN model), and

P_{32}, [m^2/m^3] the fracture intensity.

However, it should be noted that r_0 is an unknown quantity which, from all practical purposes, can be regarded as a model parameter. In fact, the choice of location parameter directly steers the fracture intensity, P_{32}, according to /Hermanson et al. 2005, Equation 3-17/:

$$P_{32,[r_{\min,new}-r_{\max,new}]} = P_{32,[r_{\min,old}-r_{\max,old}]} \frac{r_{\max,new}^{2-k_r} - r_{\min,new}^{2-k_r}}{r_{\max,old}^{2-k_r} - r_{\min,old}^{2-k_r}} \quad [1]$$

The equation simply states that if the fracture population of the model is truncated at a new lower (and/or upper) level(s), the intensity must be adjusted for accordingly. With other words, the consequence of decreasing r_0 is an increase of the number of fractures and hence an increase of the total fracture area in the model volume.

Table 2-1. The base case DFN, Forsmark version 1.2. Only the parameters of the Powerlaw distribution and the fracture intensity has been included in this study. κ = concentration of the Fisher distribution.

Set	Mean orientation of fracture poles			Size		Intensity
	Trend	Plunge	κ	k_r	r_0	P_{32}
1	87.20	1.70	21.66	2.88	0.28	0.60
2	135.20	2.70	21.54	3.02	0.25	2.07
3	40.60	2.20	23.90	2.81	0.14	0.45
4	190.40	0.70	30.63	2.95	0.15	0.23
5	342.90	80.30	8.18	2.92	0.25	0.61

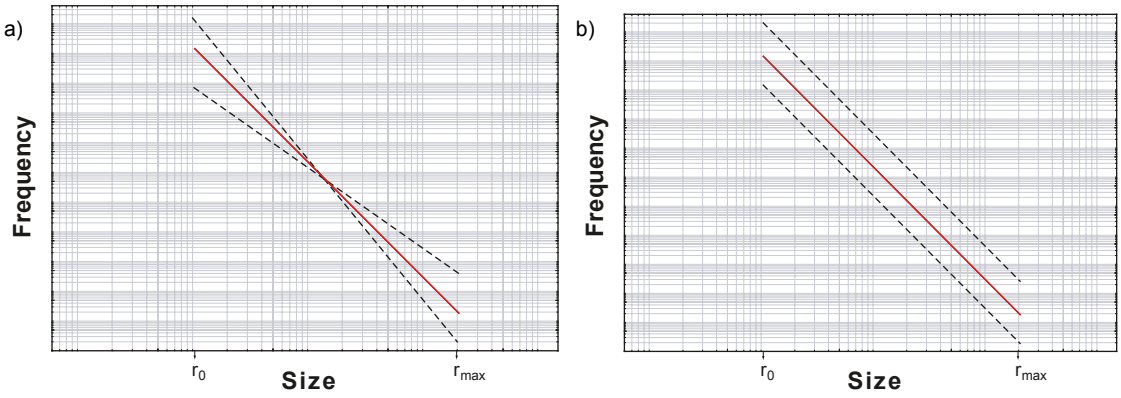

Figure 2-1. *Cartoon illustrating the results of applying weights to a) k_r and b) P_{32}.*

The consequence of decreasing k_r, the slope of the Powerlaw distribution as plotted on doubly logarithmic scales (Figure 2-1a), is to increase the relative amount of large fractures. The consequence of increasing P_{32} is, by definition, to increase the total fracture area per unit volume (Figure 2-1b).

The parameters of the DFN models were computed to simultaneously honour data in boreholes, outcrops and geophysical surveys /see e.g. Hermanson et al. 2005, for details/. The interdependency of the parameters is, naturally, fairly intricate. The immediate consequence is that, in the strictest sense, it is not possible to e.g. Monte-Carlo sample from ranges of the parameters r_0, k_r and P_{32}, for the purpose of site specific uncertainty/variability assessment, as they do not constitute truly independent entities.

Nevertheless, we here judge it feasible to treat the parameters as if they were independent for the purpose of the general sensitivity study. It should thus be understood that we use the Forsmark DFN model as a template to construct a set of hypothetical DFN models, judged to encompass a broad range of sizes and intensities combined, for the sole purpose of testing the sensitivity of the FPI criteria.

The DFN models were constructed as following:

The parameters k_r and P_{32} of the Forsmark DFN model (Table 2-1) were independently weighted using the weights [0.8, 0.9, 1.0, 1.1, 1.2] and [5.0, 2.5, 1.0, 0.4, 0.2] for k_r and P_{32} respectively. The lowest and highest weights of k_r were chosen to encompass, what is subjectively perceived by the author, fairly extreme networks. The weights of P_{32} were chosen to produce approximately the same number of fractures as produced using weighted k_r (see 3.1 for details).The adjusted values for k_r and P_{32} are displayed in Table 2-2 and Table 2-3 respectively, in which the weight "1.0", naturally, corresponds to the base case PFM v.1.2.

Table 2-2. Weighted k_r values defined by fracture set.

k_r Set#	0.8	0.9	1.0	1.1	1.2
1	2.30	2.59	2.88	3.17	3.46
2	2.42	2.72	3.02	3.32	3.62
3	2.25	2.53	2.81	3.09	3.37
4	2.36	2.66	2.95	3.25	3.54
5	2.34	2.63	2.92	3.21	3.50

Table 2-3. Weighted P_{32} values defined by fracture set.

P_{32} Set#	5.0	2.5	1.0	0.4	0.2
1	3.01	1.51	0.60	0.24	0.12
2	10.35	5.17	2.07	0.83	0.41
3	2.24	1.12	0.45	0.18	0.09
4	1.13	0.57	0.23	0.09	0.05
5	3.03	1.51	0.61	0.24	0.12

From Table 2-3 and Table 2-2 it is possible to construct a large number (124) of DFN models, in addition to the base case (weight = 1) by combining k_r and P_{32} for different fracture sets. Due to the immense computation demands, roughly 3–6 hours per model (500 realisations each), we restricted the range using weights for P_{32} and keeping k_r fixed to the base case and, similarly, using weights of k_r, using P_{32} of the base case. Additionally, we used the same weight for all fracture sets, to reduce the number of models further. This procedure resulted in 8 DFN models in addition to the base case. We also included the Laxemar v.1.2 model for reference. These constitute the base models used for studying the sensitivity to DFN parameters. To study the effect of modelling assumptions two additional models were constructed: one model in which we take account for varying amount of slip along a fracture and one model that take account for intersections with neighbouring tunnels. Further, to test the FPI simulations against an analytical benchmark, yet another one model was constructed in which random fracture orientations are assumed (by setting Fisher $\kappa < 0.1$). Thus, a total of 13 different DFN models have been analysed.

We used an upper radius limit of 250 m and the dimensions (in m) of the models were:

x = 500

y = 250

z = 250.

We provide realisation samples of each base model variant in Figure 2-2 to Figure 2-4. The samples represent intersections of circular discs on 50×50 m, horizontal sampling surfaces. The models only included fracture radii larger than or equal to 3.09 m (see also 3.1). Red lines represent *traces* larger than 25 m.

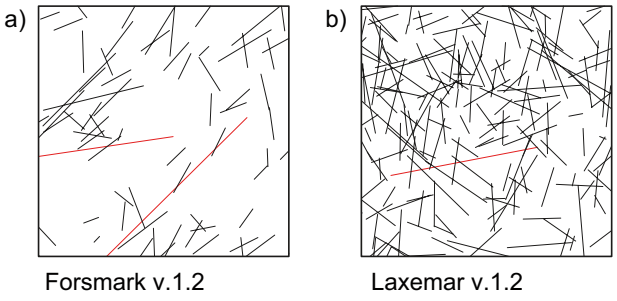

Figure 2-2. *Fracture traces using the Forsmark v.1.2 (a) and Laxemar v.1.2 (b) DFN models.*

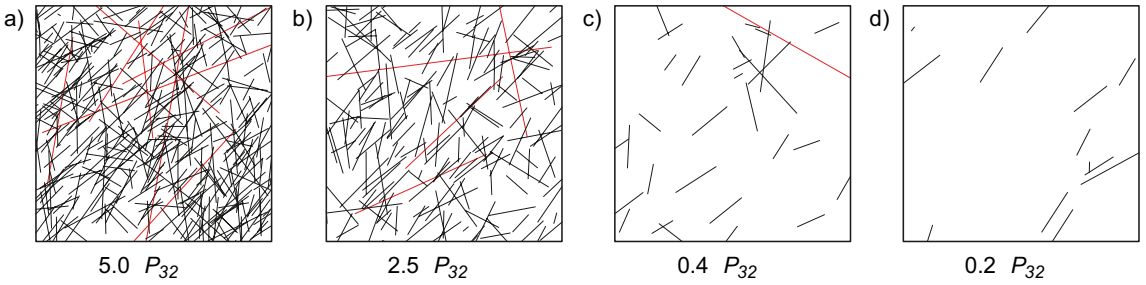

Figure 2-3. *Fracture traces using P_{32}-weighted variants of the base case.*

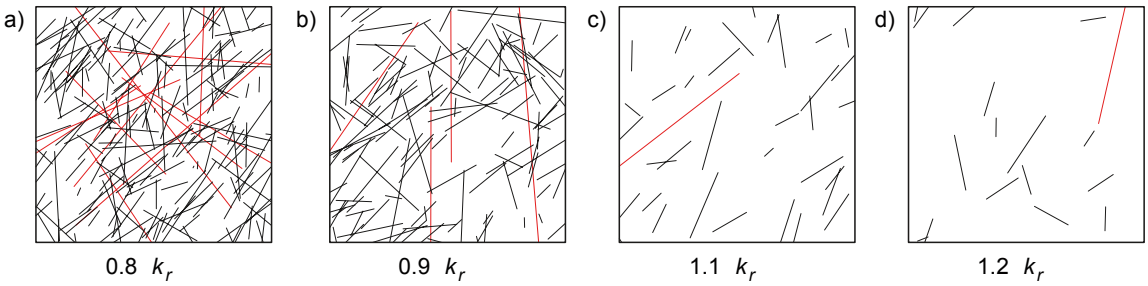

Figure 2-4. *Fracture traces using k_r-weighted variants of the base case.*

3 Results

3.1 Number of fractures

Naturally, the factor that has the largest impact upon the FPI criteria is the number of large fractures in the rock volume. However, the total number of fractures produced by the various DFN models is the result of an intricate interplay between the different DFN parameters. For a given intensity, the model can either contain a few very large fractures or many much smaller ones.

The number of fractures per unit volume, P_{30}, can be computed using the following expression:

$$P_{30} = \frac{N}{V} = \frac{P_{32}}{\pi \int_{r_0}^{\infty} r^2 f(r)\, dr} \qquad [2]$$

In which N is the number of fractures, V the model volume, $f(r)$ the probability density distribution of fracture sizes for a particular fracture set and P_{32} the intensity of fractures in the size range [r_0 – inf[1]].

For the subset of fractures within the range $r_{min} < r < r_{max}$, P_{10} can be rescaled using /see e.g. Munier 2006, for details/:

$$P_{30,rescaled} = \frac{P_{32}}{\pi \int_{r_0}^{\infty} r^2 f(r)\, dr} \int_{r_{min}}^{r_{max}} f(r)\, dr \qquad [3]$$

For example, applying equation [3] on the model variant "0.8 k_r", roughly 100 million fractures are predicted within the 500×250×250 m^3 simulation volume (r_0, r_{max} = 250). Naturally, such an overwhelming number of fractures would impose an unnecessary computation burden since the only fractures of interest are those capable of intersecting the full perimeter of the tunnel. The model had a tunnel cross-sectional area of 30 m^2, which corresponds to a radius of roughly 3 m. Due to the powerlaw, the number of fractures in the range r_0 – 3.09 m is huge so the number of fractures that are actually modelled is very much less. We therefore used a minimum fracture radius, r_{min}, corresponding to the radius of the tunnel (3.09) and adjusted P_{32} accordingly.

An additional complication is that the expanded FPI criterion (EFPC) only makes use of fractures capable of intersecting 5 deposition holes or more /see e.g. Munier 2006, for details/. Using a spacing of 6 m between deposition holes the radius of such a fracture, if ideally oriented for intersection, is 12 m thus reducing the number of simulated fractures further. Figure 3-1 summarises the number of simulated fractures in each base model variant (using r_{min} = 3.09).

[1] It should be noted that in some contexts, the upper truncation is steered by a chosen limit between deterministic and stochastic modelling. In most site descriptions, this limit was chosen to approximately 1,000 m trace length, i.e. corresponding to a radius of 564 m.

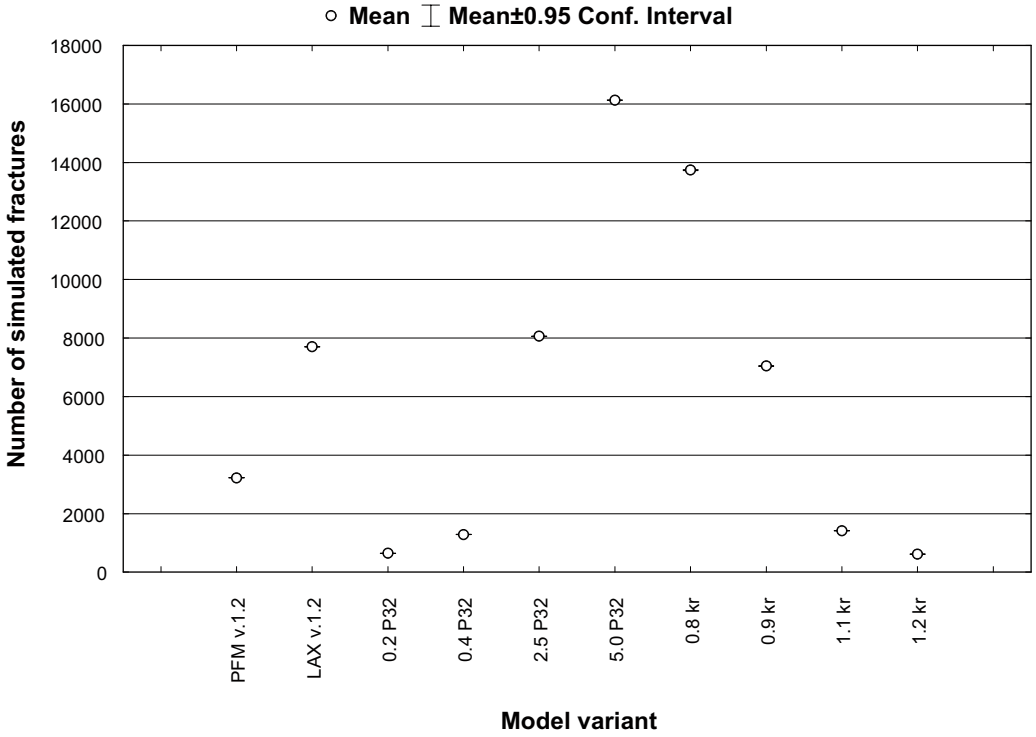

Figure 3-1. *Number of simulated fractures in each model variant.*

3.2 Number of full perimeter intersections

3.2.1 Analytical benchmark

To test that the algorithms which computes the cylinder-plane intersections performs as intended, a couple of semi-analytical benchmarks /Dershowitz 1985, Wang 2005/ were setup.

The first benchmark assumes uniform orientations of the discs. If the discs are perpendicular to the tunnel axis, the number of FPI per unit length (P_{10} for an infinitely thin cylinder) should equal the fracture intensity P_{32}. A uniform orientation distribution was mimicked by setting the Fisher κ to 150 (Table 3-1).

A second benchmark assumes random orientations of the discs. The predicted number of FPI per unit length (P_{10} for an infinitely thin cylinder) is:

$$P_{10} = \frac{P_{32}}{2} \qquad [4]$$

The simulated fracture intensities, using the parameters in Table 3-1 and 500 realisations, are displayed in Figure 3-2. Simulated P_{32} of the models agree very well with those predicted by equation [1]. From this, we conclude that the powerlaw size distribution, the number of fractures and the nested model volumes are adequately implemented in the simulation algorithms.

The sampled P_{10} values, i.e. the number of FPI per unit tunnel length (using a very thin tunnel), also agree very well with those predicted by equation [4] (Figure 3-3). We attribute the small discrepancy between predicted and observed P_{10} values to the finite size of the tunnel. We were, unfortunately, not able to simulate even smaller tunnel radii without encountering numerical oddities. Nevertheless, from this we still conclude that the algorithms that compute the intersection between a tunnel and a disc performs as intended.

Table 3-1. Parameters used for benchmarking the cylinder-disc intersection algorithm.

Parameter	Value
Tunnel radius:	0.0001 m
r_{max}	250 m
r_{min}	50 m
r_0	50 m
Tunnel trend	90°
Tunnel plunge	0°
Fracture mean trend (normals)	90°
Fracture mean plunge (normals)	0°
k_r	2.9
P_{32} [50-inf]	5 m^2/m^3
P_{30} [50-inf]	1.975717E–4 m^{-1}
Predicted $P_{32, rescaled}$ [50–250] (using equation [1])	3.825381
Predicted $P_{30, rescaled}$ [50–250] (using equation [3])	1.957151E–4 m^{-1}
Fisher κ, random orientations	0.01
Fisher κ, uniform orientations	150

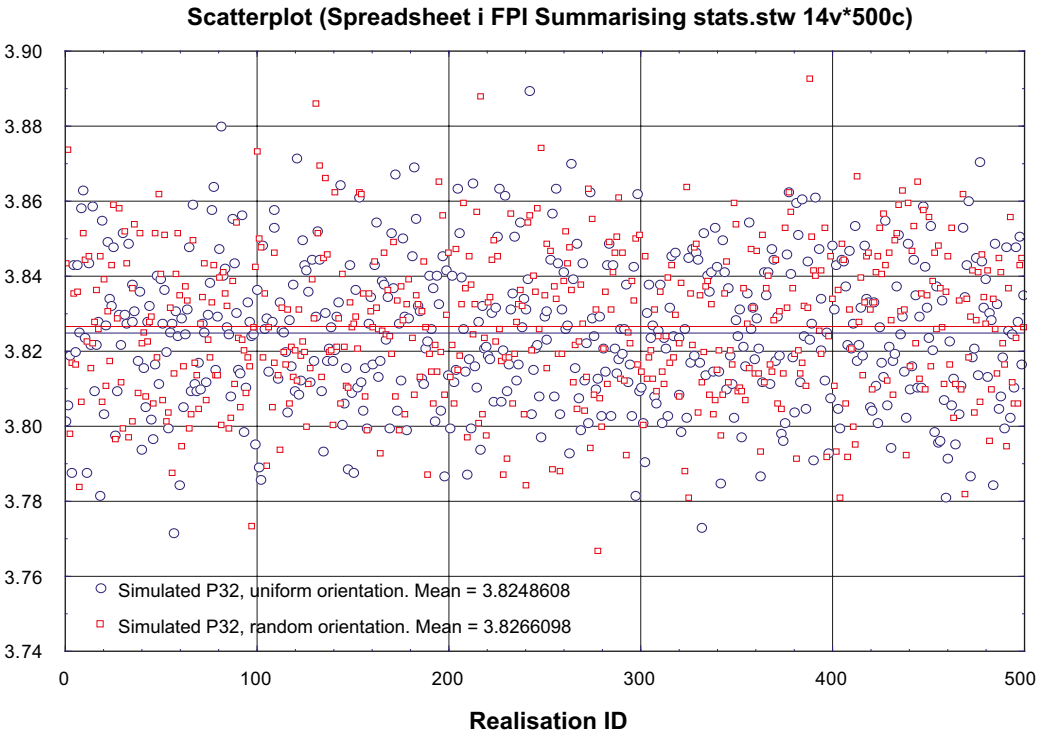

Figure 3-2. *Simulated intensities (P_{32}).*

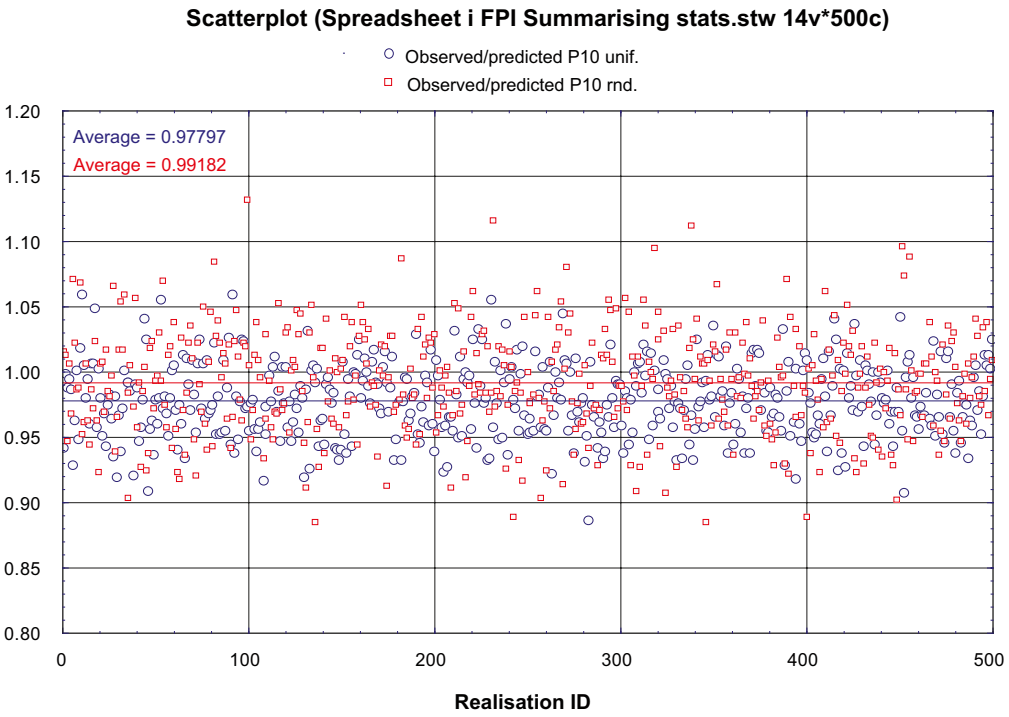

Figure 3-3. *Benchmark of the cylinder-plane intersection algorithm.*

3.2.2 Simulations

The starting point of the simulations is to identify each FPI in the deposition tunnel and then to extrapolate the fracture plane to eventual intersection with one or several deposition holes. Expectedly, the difference in number of FPIs between the model variants (Figure 3-4) basically mimics the difference in number of fractures in the model (Figure 3-1).

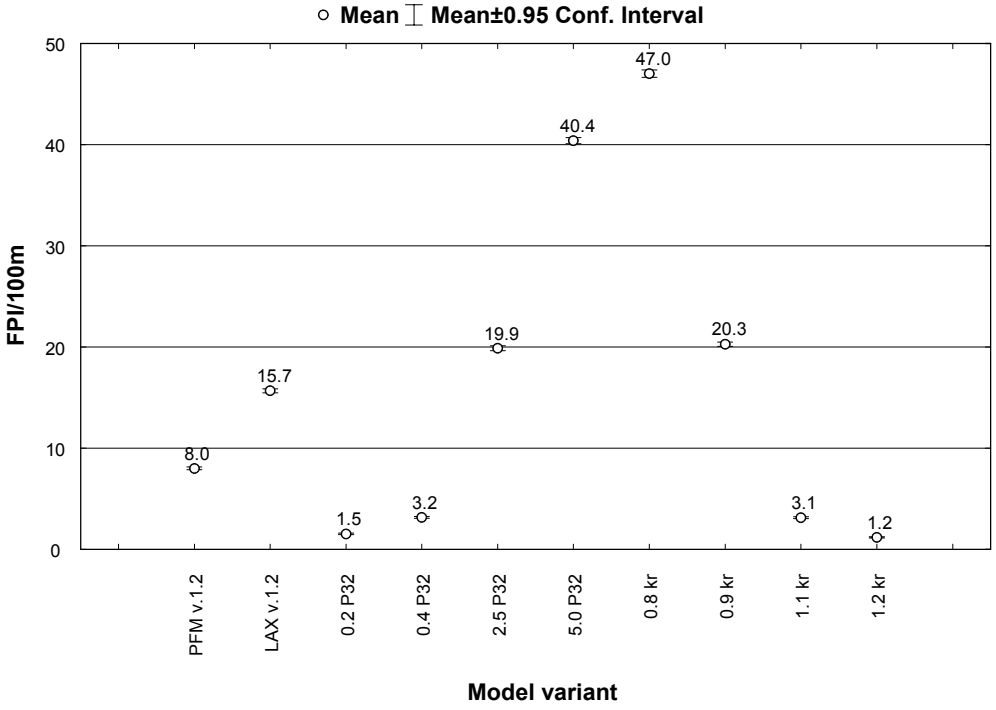

Figure 3-4. *Number of full perimeter intersections (FPI) per 100 m deposition tunnel using various model variants. Each model variant corresponds to 500 realisations.*

It should be noted that the number of predicted FPI using the Laxemar 1.2 DFN roughly amounts to 16 per 100 m. This is in a very good agreement with the number of FPI mapped in the nearby Äspö HRL (Figure 3-5).

3.3 Undetected critical positions

The success of EFPC to detect large fractures depends largely upon the restrictions imposed on the criterion. Unless we expand the criterion to cover FPI also in all deposition holes, which would render completely unrealistic degree-of-utilisation (see 3.3.1), there will always be a small portion of fractures that escapes the detection criterion.

To warrant the integrity of canisters in the case of a large nearby earthquake, we introduced the notion of respect distance /Munier and Hökmark 2004/. In short, no canisters are to be emplaced closer to a deformation zone than 100 m from its boundary. /Munier and Hökmark 2004/ argued that within the distance 100–200 m from a deformation zone (Figure 3-6) capable of hosting an earthquake of magnitude 6 or larger, a fracture must have a radius exceeding 75 m to host a slip exceeding the canister failure criterion. /Fälth and Hökmark 2006/ showed that, for distances beyond 200 m from an earthquake generating deformation zone, fractures must have radii exceeding 150 m to be able to host a damaging slip. As the intersection probabilities differ between these fracture classes, they needed to be analysed separately in terms of EFPC efficiencies.

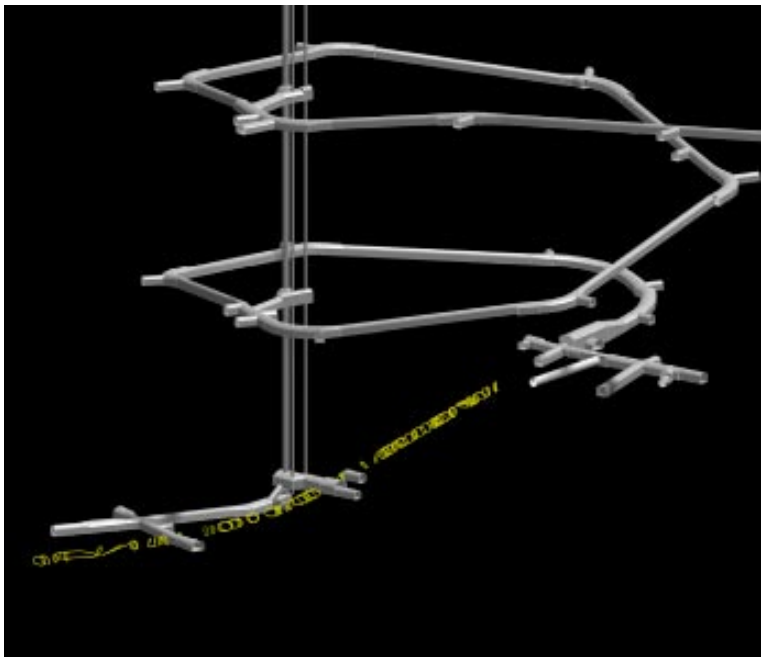

Figure 3-5. *The TBM part of the Äspö HRL hosts roughly 17 FPI per 100 m tunnel.*

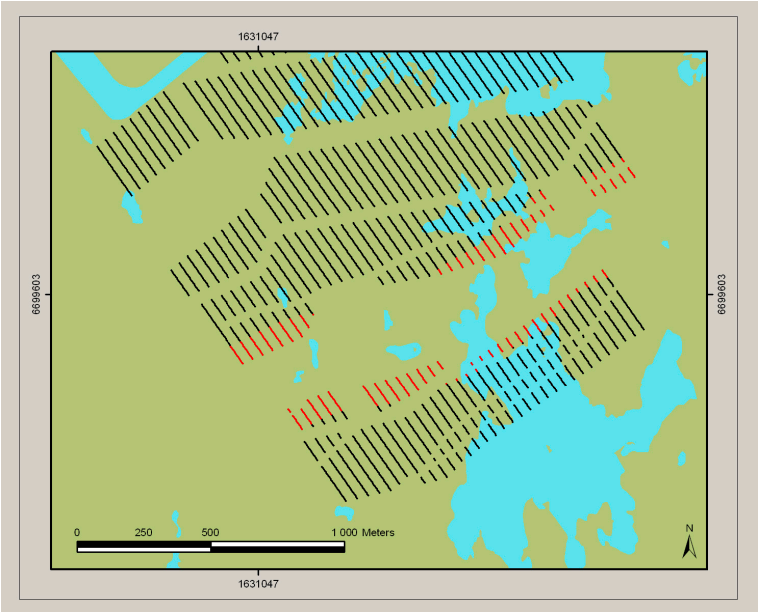

Figure 3-6. *Deposition holes within the 100–200 m band of deformation zone ZFMNE0060 (in red) at Forsmark (depth = –400 m) Layout from /Brantberger et al. 2006/.*

Though some deposition *holes* escapes the EFPC criterion, it should be noted that very few *fractures* escapes the criterion. In fact, of all 500 realisations of the base case, which corresponds to 4.25 complete repositories, only one realisation had more than one escaping fracture. This corresponds to roughly 117 undetected critical *fractures* per repository. Each of these transected between 1 and 4 deposition holes that escaped the detection criteria (Figure 3-7).

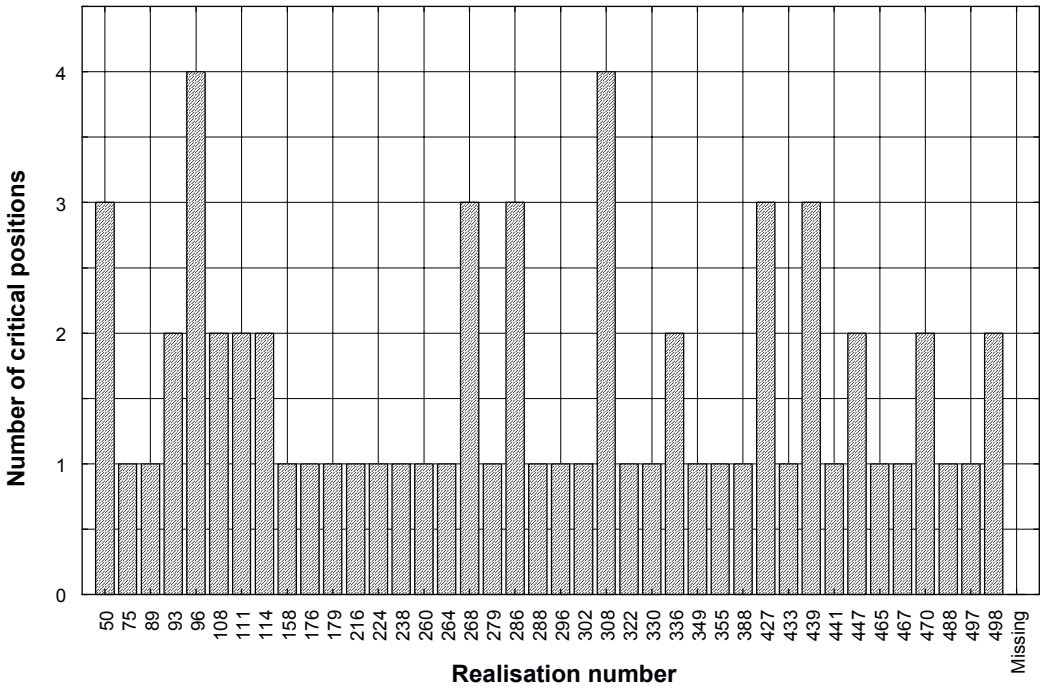

Figure 3-7. *Number of critical deposition holes that escaped the criteria per realisation, base case (PFM v.1.2, 300 m deposition tunnel).*

3.3.1 Measure of efficiency of the EFPC criterion

Using the procedures of /Hedin 2005/, we computed the fraction of deposition holes that, on average, are intersected by fractures with radii exceeding 75 and 150 m respectively for each model variant (Figure 3-8).

This measure, denoted ε*Design*, is used to compute the efficiency of the EFPC criterion. We formulate the efficiency, *E*, as:

$$E = \frac{(\varepsilon Design \cdot N) - n}{\varepsilon Design \cdot N} \qquad [5]$$

were *n* is the number of intersected deposition holes that escaped the EFPC criterion and *N* the total number of deposition holes in the model (6,000).

Computed mean efficiencies (Figure 3-9) do not differ much between the modelled DFN variants. In fact, it is not possible to demonstrate any statistically valid difference at the 95% confidence level between any of the analysed variants though we note that the mean values range between roughly 90% and 98%.

The efficiency of the criterion is, however, associated to an expense; the degree-of-utilisation. Expectedly, the degree-of-utilisation is the lowest for the smallest weights of k_r and lowest for the largest weights of P_{32}. The reader is kindly referred to /Munier 2006/ for details regarding the computation of degree-of-utilisation.

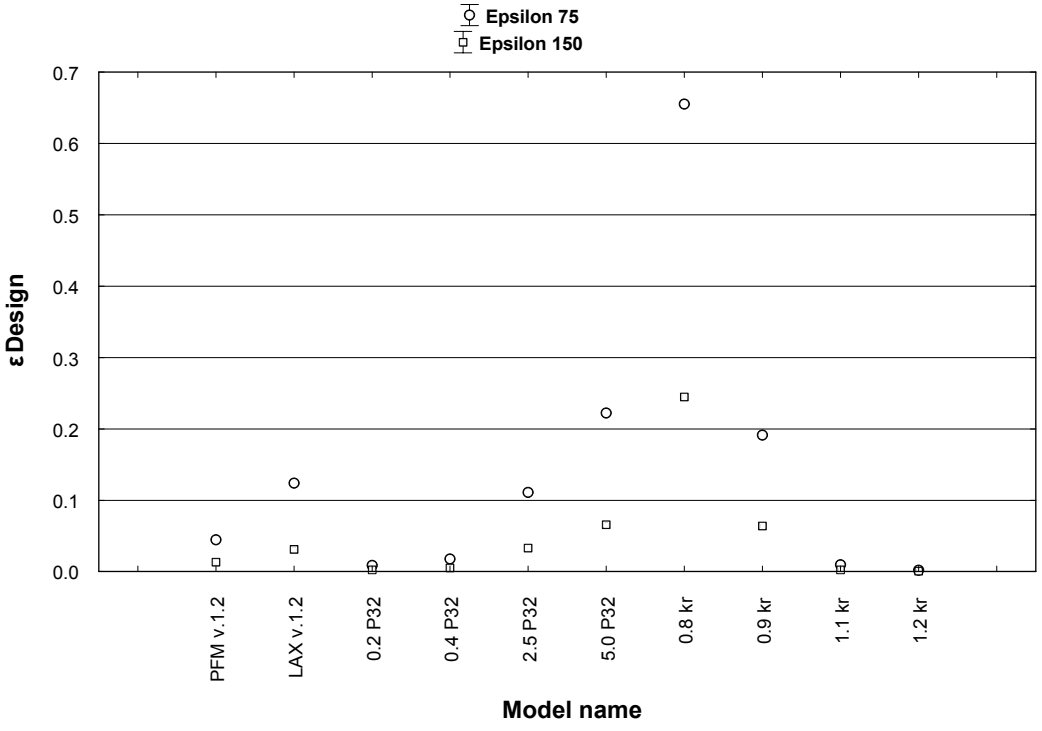

Figure 3-8. *The fraction (εDesign) of the canister holes that are intersected by fractures with radii exceeding 75 and 150 m.*

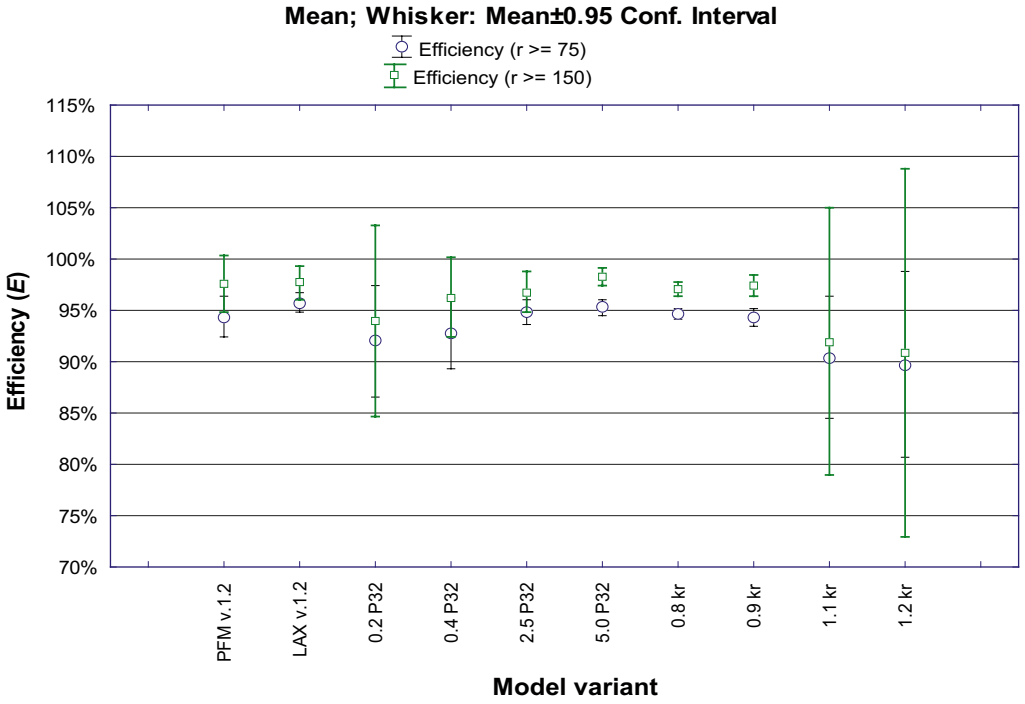

Figure 3-9. *Efficiencies of the EFPC criterion for various model variants.*

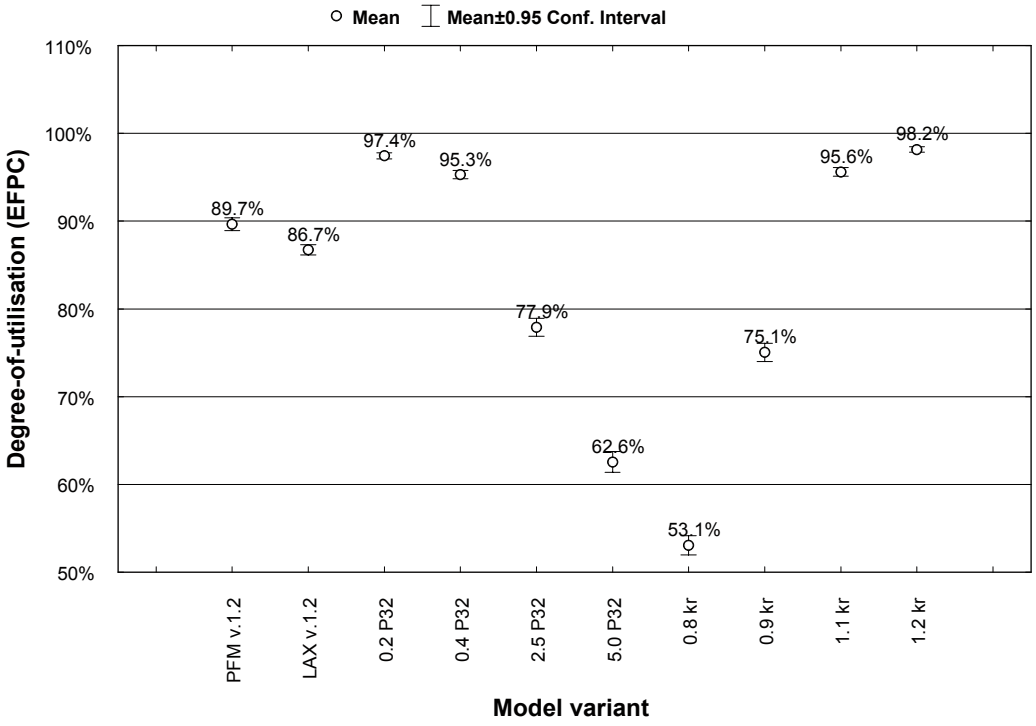

Figure 3-10. *Degree-of-utilisation using EFPC for various model variants.*

3.3.2 Effect of simulating only one tunnel

As discussed in /Munier 2006/, fractures that escape detection are typically large fractures located in the ends of the "deposition tunnel" (Figure 3-11). From an FPI perspective, the deposition tunnels are joined to transportation tunnels that will also be mapped. As transportation and neighbouring deposition tunnels were not included in the simulations, the number of critical deposition holes that escaped the EFPC criterion is considerably higher than we would expect using additional information from neighbouring tunnels. It should be noted, though, that such fractures will most probably be detected underground by other means /Cosgrove et al. 2006/ in addition to using the FPI criteria. The number of undetected, critical, deposition holes provided by Figure 3-12 is thus a cautious overestimation.

If it is reasonable to assume that such fractures will in fact be detected as FPI in neighbouring tunnels, then the number of undetected, critical, deposition holes reduces dramatically as shown in Figure 3-13. For fractures of 150 m and larger, the detection success is 100%.

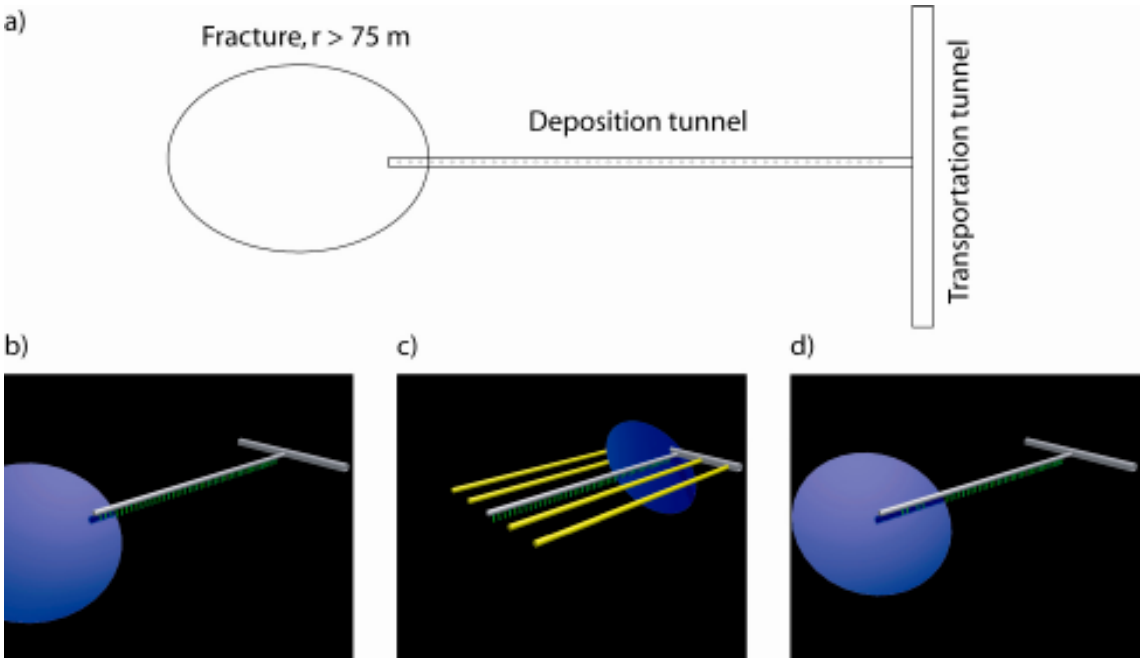

Figure 3-11. *A fracture intersecting the end of the deposition tunnel, thereby escaping the EFPC criterion (a, b). Many fractures intersect either the transportation tunnel or neighbouring deposition tunnels (c). Some fractures escape detection simply as an artefact of the simulation sequence (d, see also 3.3.3).*

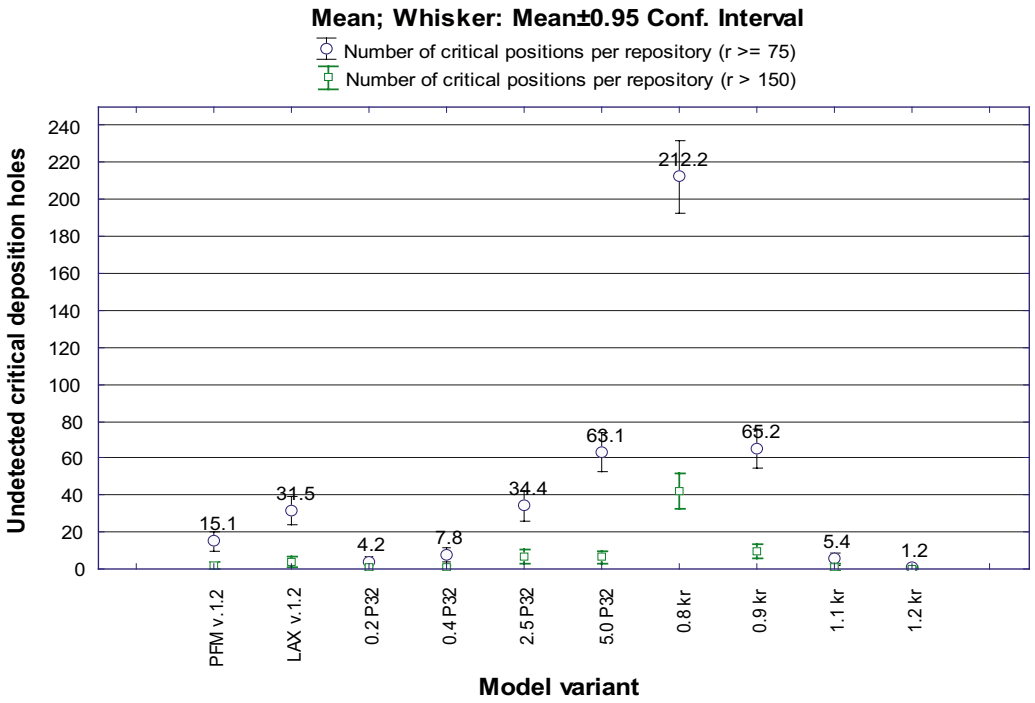

Figure 3-12. *Number of undetected, critical deposition holes that escaped the EFPC criterion (6,000 canister repository).*

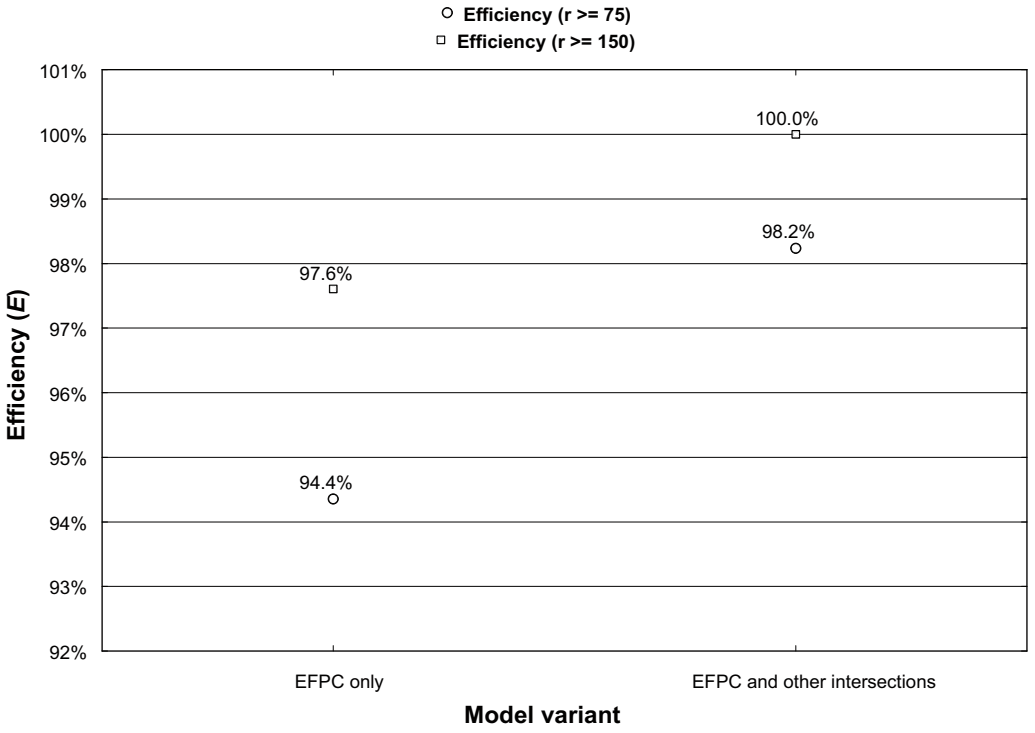

Figure 3-13. *The graph shows that if account is taken for intersection with neighbouring tunnels, the efficiency of the criteria increases considerably.*

3.3.3 Effect of simulation sequence

The simulation sequence was set up to mimic, to the furthest possible extent, the mapping procedure anticipated in the tunnels. We therefore assumed the following:

1. Deposition tunnels are mapped and modelled in 3D.
2. Unsuitable positions are disregarded. This would include an application of FPC.
3. The preliminary accepted positions are probed by means of cored drilling.
4. Unsuitable positions are disregarded. This would include an application of EFPC.
5. Depositions holes are drilled.
6. Unsuitable positions are disregarded. This would, again, include an application of EFPC.

Some critical deposition holes escape the EFPC criterion simply as an artefact of the simulation sequence (Figure 3-14). This is because the deposition holes would have fulfilled the EFPC criterion if some of them were not already rejected by the previous FPC criterion. By reversing the simulations, i.e. starting with EFPC rather than FPC, the number of escaped positions will be reduced.

This reasoning is not merely concerning the structure of the computer-code. The analogue in a real situation would be to:

1. regularly probe the deposition tunnels with boreholes, regardless of the outcome of the FPC,
2. use crosshole tomography and other techniques to apply the EFPC criterion,
3. apply FPC on the remaining positions,
4. drill deposition holes where acceptable,
5. eventually reject any unsuitable deposition holes.

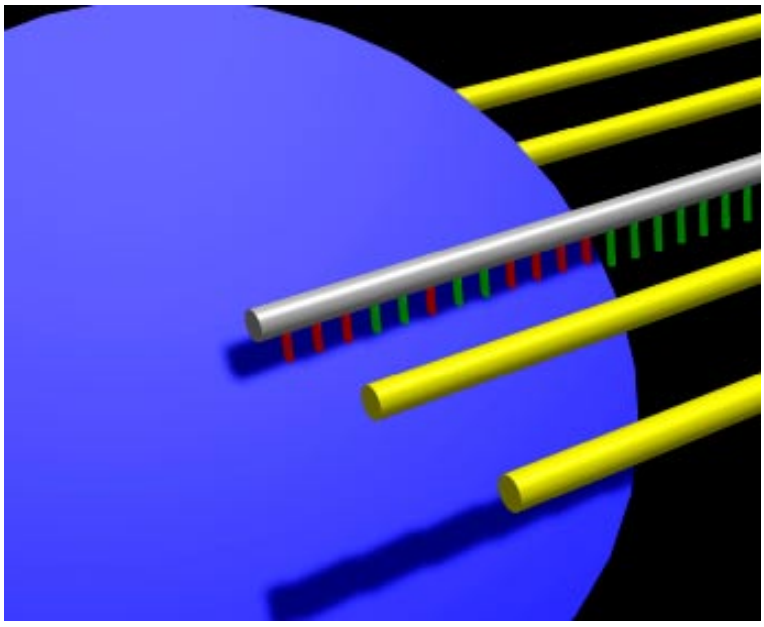

Figure 3-14. *The figure illustrates how a large fracture can escape the EFPC criterion as an artefact of the simulation procedure (detail from Figure 3-11d). Deposition holes identified by FPC are shown in red. As these are already excluded the remaining number of deposition holes is insufficient to fulfil the EFPC criterion of 5 or more consecutive intersections.*

SKB is currently detailing deposition hole acceptance criteria and the mapping procedure has not yet been established. Assuming a mapping procedure without regular probing would thus constitute a cautious overestimation of the number of critical positions that escaped both criteria.

3.3.4 Effect of varying slip along the fracture

For a linear elastic medium, the displacement profile along a fracture of radius r varies from d_{max} at the center ($r' = 0$) to zero at the fracture tip ($r' = r$) according to /ITASCA 2004/:

$$\frac{d_{r'}}{d_{\max}} = \sqrt{1-\left(\frac{r'}{r}\right)^2} \qquad [6]$$

This means that d_{crit} occurs at a distance r'_{crit} given by:

$$r'_{crit} = r\sqrt{1-\left(\frac{d_{crit}}{d_{\max}}\right)^2} = r\sqrt{1-\left(\frac{r_{\min}}{r}\right)^2} = \sqrt{r^2 - r_{\min}^2} \quad r > r_{\min} \qquad [7]$$

In the simulations presented here, we have assumed that fractures with radii larger than 75 m are able to host slip exceeding the canister failure criterion, 0.1 m. Thus r_{min} = 75 m. To exploit the effect of taking varying slip along a fracture into account, we rescaled all fractures (r > 75 m) of the base case according to [7], prior to applying the EFPC criterion. That is, only the part of the fracture that can host a slip exceeding the canister failure criterion is included in the EFPC simulations. The implication is the following: Even if a deposition hole is intersected by a critical fracture, the integrity of the canister will not be jeopardised as long as the intersection point is not too close to the centre of the fracture were the slip is the largest.

Figure 3-15 shows an example of a fracture that escaped EFPC and that still jeopardise the canister integrity despite taking account for decaying slip towards the tip. In a total of 500 realisations, seven fractures were still regarded discriminating after having taken account for slip. This would correspond to 1.7 such fractures per repository volume.

The increase in efficiency is dramatic as shown on Figure 3-16. By, additionally, combining the effect of decaying slip with the possibility of detecting the fractures in neighbouring tunnels, the efficiency is increased further, to almost 100% for all relevant fractures. It should be noted that the realisation shown on Figure 3-15 is the only one out of 500 in which the fracture do not intersect neighbouring tunnels. This would correspond to 0.23 such fractures per repository on average.

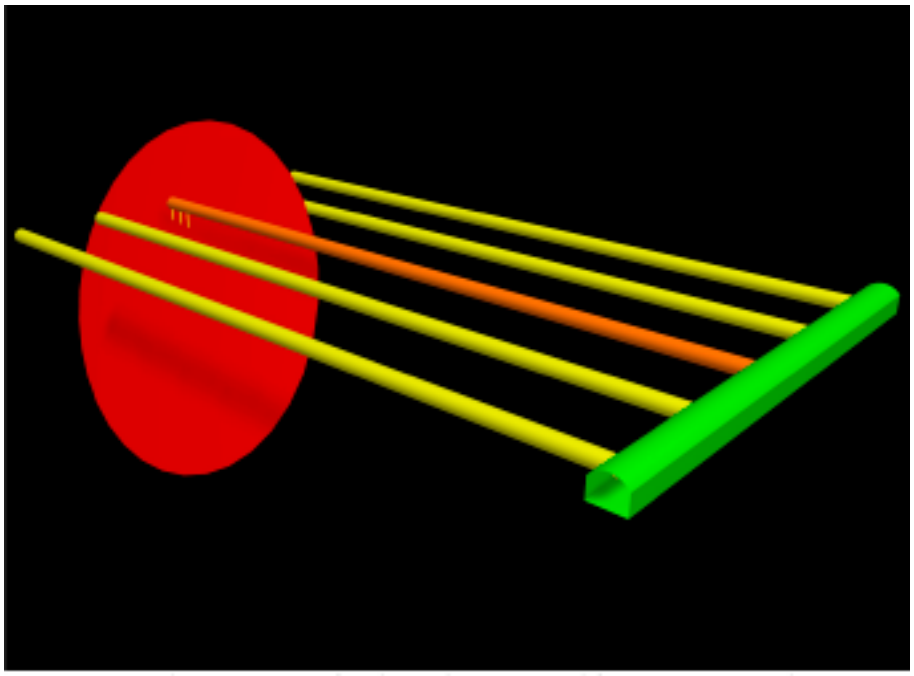

Figure 3-15. *When accounting for slip, only one critical fracture in 500 realisations intersected 4 deposition holes*[2].

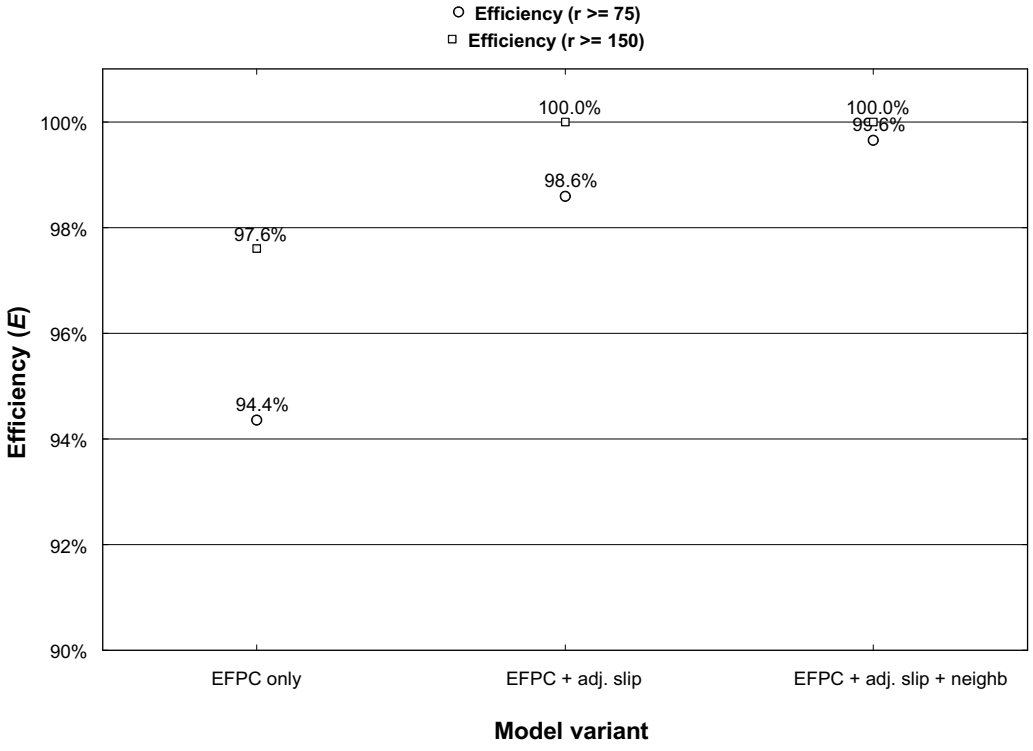

Figure 3-16. *The graph shows that if account is taken for decaying slip towards the fracture tip, the efficiency of the criteria increases considerably. If, additionally, account is taken for intersection with neighbouring tunnels, the efficiency is almost 100% for all fractures of relevance.*

[2] The complete output from all realisations is available from the author upon request. This particular fracture/tunnel configuration resulted from realisation # 459, model "slip adjust".

4 Conclusions

The impact of DFN uncertainty upon the EFPC criterion was evaluated, to assess its potential importance on safety assessments. We performed numerous simulations using variants of the Forsmark 1.2 DFN, to address the impact of various DFN parameters.

The most important conclusion of this study is that the efficiency of the EFPC is high for all tested model variants. That is, compared to blind deposition, the EFPC is a very powerful tool to identify unsuitable deposition holes and it is *essentially insensitive to variations in the DFN Model*. If information from adjacent tunnels is used in addition to EFPC, then the *probability of detecting a critical deposition hole is almost 100%.*

In addition, we conclude the following:

- The number of FPI is governed by the intensity of fractures in the size range 3.09-250 m. This intensity can be altered by either altering the overall intensity, P_{32}, by altering the shape parameter of the powerlaw, k_r, or both.
- Lower k_r values render more unfavourable conditions than higher k_r, as compared to the base case. The increase of intensity in the critical size range is manifested as a higher number of FPI per tunnel length and, utterly, a higher number of deposition holes intersected by potentially critical structures (higher ε). It should be noted, however, that the uncertainty in the estimation of k_r from site data would most certainly provide a much narrower range than the weights used in this sensitivity analysis.
- The number of deposition holes that escaped the EFPC criterion is also governed by the shape parameter, k_r. This is because fractures applicable to the EFPC criterion, $r \geq 12$ m in the current application, increase in relative amount with decreasing k_r, hence increasing the intersection probability. It should be noted, though, that the number of positions that escapes the criterion can be substantially reduced by using a more restrictive limit of the number of allowed intersections (≥ 5 intersected positions in the current application), however to the expense of a lower degree of utilisation.
- Very low values of k_r, which yield high values of P_{32} in the critical size range, renders unacceptably low degrees-of-utilisation and too many missed critical deposition holes. It should be noted, though, that even for the most extreme DFN variant, the degree-of-utilisation exceeds 50%.

5 References

Brantberger M, Zetterqvist A, Arnbjerg-Nielsen T, Olsson T, Outters N, Syrjänen P, 2006. Final repository for spent nuclear fuel. Underground design Forsmark, Layout D1. SKB R-06-34, Svensk Kärnbränslehantering AB.

Cosgrove J, Röshoff K, Stanfors R, 2006. Geological characteristics of deformation zones and strategy for their detection. SKB R-06-39, Svensk Kärnbränslehantering AB

Darcel C, Davy P, Bour O, De Dreuzy J R, 2004. Alternative DFN model based on initial site investigations at Simpevarp. SKB R-04-76, Svensk Kärnbränslehantering AB.

Dershowitz W, 1985. Rock Joint System. Cambridge, Mass., MIT. Ph.D.

Fälth B, Hökmark H, 2006. Seismically induced shear displacement on repository host rock fractures. Results of new dynamic discrete fracture modeling. SKB R-06-48, *in prep*, Svensk Kärnbränslehantering AB.

Hedin A, 2005. An analytic method for estimating the probability of canister/fracture intersections in a KBS-3 repository. SKB R-05-29, Svensk Kärnbränslehantering AB.

Hermanson J, Forssberg O, Fox A L P P, 2005. Statistical model of fractures and deformation zones. Preliminary site description, Laxemar subarea, version 1.2. SKB R-05-45, Svensk Kärnbränslehantering AB.

ITASCA, 2004. UDEC, Universal Distinct Element Code. 3.1, users manual. ITASCA conclusting group Inc.

La Pointe P R, Olofsson I, Hermanson J, 2005. Statistical model of fractures and deformation zones for Forsmark. Preliminary site description Forsmark area - version 1.2. SKB R-05-26, Svensk Kärnbränslehantering AB.

Munier R, Hökmark H, 2004. Respect distances. Rationale and means of computation. SKB R-04-17, Svensk Kärnbränslehantering AB.

Munier R, 2006. Using observations in deposition tunnels to avoid intersections with critical fractures in deposition holes. SKB R-06-54, Svensk Kärnbränslehantering AB.

Wang X, 2005. Stereological interpretation of rock fracture traces on borehole walls and other cylindrical surfaces. Balcksburg, Virginia, Virginia Polytechnic Institute and State University. PhD.